Author/s:
Rahim, MA;Kempe, K;Müllner, M;Ejima, H;Ju, Y;Van Koeverden, MP;Suma, T;Braunger, JA;Leeming, MG;Abrahams, BF;Caruso, F

Title:
Surface-Confined Amorphous Films from Metal-Coordinated Simple Phenolic Ligands

Date:
2015-08-25

Citation:
Rahim, M. A., Kempe, K., Müllner, M., Ejima, H., Ju, Y., Van Koeverden, M. P., Suma, T., Braunger, J. A., Leeming, M. G., Abrahams, B. F. & Caruso, F. (2015). Surface-Confined Amorphous Films from Metal-Coordinated Simple Phenolic Ligands. Chemistry of Materials, 27 (16), pp.5825-5832. https://doi.org/10.1021/acs.chemmater.5b02790.

Surface-Confined Amorphous Films from Metal-Coordinated Simple Phenolic Ligands

Md. Arifur Rahim,[†] Kristian Kempe,[†,§] Markus Müllner,[†,#] Hirotaka Ejima,[†,¶] Yi Ju,[†] Martin P. van Koeverden,[†] Tomoya Suma,[†] Julia A. Braunger,[†] Michael G. Leeming,[‡,∥] Brendan F. Abrahams,[‡] and Frank Caruso*[,†]

[†]ARC Centre of Excellence in Convergent Bio-Nano Science and Technology, and the Department of Chemical and Biomolecular Engineering, The University of Melbourne, Parkville, Victoria 3010, Australia

[‡]School of Chemistry, The University of Melbourne, Parkville, Victoria 3010, Australia

[∥]Bio21 Institute of Molecular Science and Biotechnology, The University of Melbourne, Parkville, Victoria 3010, Australia

ABSTRACT: Coordination chemistry of natural polyphenols and transition metals allows rapid, self-assembly of conformal coatings on diverse substrates. Herein, we report that this coordination-driven self-assembly process applies to simple phenolic molecules with ditopic or monotopic chelating sites (as opposed to macromolecular, multitopic polyphenols), leading to surface-confined amorphous films upon metal coordination. Films fabricated from gallic acid, pyrogallol, and pyrocatechol, which are the major monomeric building blocks of polyphenols, have been studied in detail. Pyrocatechol, with one vicinal diol group (i.e., bidentate), has been observed to be the limiting case for such assembly. This study expands the toolbox of available phenolic ligands for the formation of surface-confined amorphous films, which may find applications in catalysis, energy, optoelectronics, and biomedical sciences.

INTRODUCTION

Modular control over the rational design of supramolecular architectures has been achieved in the last two decades by smart engineering of coordination-driven self-assembly processes.[1] Early prediction of the inherent preferences for directionality and binding affinity within the complementary building blocks of coordination complexes has paved the way for fabricating structures with extended networks of metal clusters bridged by compatible organic ligands.[2,3] Porous coordination polymers or metal-organic frameworks (MOFs) with distinct spatial and geometrical arrangements of the interconnecting motifs are examples of such organic-inorganic hybrid materials.[4-7] These crystalline materials with structurally encoded nano- and micro-porosities have potential application for gas storage, separation and sensing.[8-13] On the other hand, surface-bound or freestanding amorphous thin films/coatings are another class of network materials of importance in several branches of science,[14-16] where polymeric (covalent) compounds are the predominantly used structural components. Research has also focused on exploring novel strategies to incorporate inorganic moieties in polymeric films to obtain hybrid functional materials that exploit the synergistic effects of the organic and inorganic constituents.[17,18] In this context, processes utilizing self-assembly of coordination complexes are a promising strategy toward facile engineering of thin films with defined properties.

Recently, we reported a facile assembly approach that exploits polyphenol-metal interactions, specifically between tannic acid (TA) and iron(III) (Fe^{III}) ions, to form thin films.[19] Our interest in these metal-polyphenol systems arises from the facile and versatile nature of the assembly process, to produce tunable, dynamic materials. Using TA as a versatile ligand, we demonstrated the formation of capsules with engineered pH-responsive degradation, luminescence and positron emission, by judicious choice of the incorporated metal,[20] as well as pH-responsive drug delivery vectors[21] and cytoprotective coatings.[22] Furthermore, we reported the assembly of Fe^{III}-polyphenol capsules from a synthetic poly(ethylene glycol)-based polyphenol, which exhibited reduced protein fouling and non-specific cellular association compared to TA/Fe^{III} capsules.[23] For the TA systems, initiation of the film assembly is likely to occur by adsorption of TA to the surface and subsequent strong intermolecular (and possibly intramolecular) crosslinking by the metal ions. Film formation was rationalized by the strong affinity of polyphenols for various surface chemistries, and the polymeric, multitopic structure of TA containing multiple galloyl groups covalently attached to a central glucose core. However, whether the amorphous nature of the films originates from the asymmetry of TA or from a generic interfacial behavior of metal-phenolic ligand interactions is unclear. MOF synthesis studies show that simple ditopic or tritopic ligands, even with symmetric binding sites, can produce stable kinetically trapped amorphous phases (byproduct or major product) in bulk depending on the choice of ligand/metal pair and synthetic conditions.[1,3,24-27] It remains to be determined whether the amorphous network of TA and metal ions formed on surfaces is limited to polyphenols (i.e., multiple binding/chelating sites with structural asymmetry) or is more a generic phenomenon

(i.e., kinetic assembly) that can be expanded to simple phenolic ligands with few binding/chelating sites.

In our effort to understand these types of metal-phenolic systems, we have discovered that phenolic ligands containing single aromatic rings with ditopic or monotopic chelating groups are also able to form continuous films on solid surfaces through coordination interactions with metal ions. Each of the phenolic ligands, namely gallic acid (GA), pyrogallol (PG) and pyrocatechol (PC), resulted in instantaneous film formation on substrate surfaces upon coordination with Fe^{III} ions. Network/film formation by these simple ligands is discussed in detail considering different interactions and growth conditions. From structural considerations of the diverse library of phenolics, it can be concluded that at least one vicinal diol group (bidentate) is essential to form an amorphous film, leaving PC as the limiting case for such phenolic-metal assemblies.

EXPERIMENTAL SECTION

Materials. Gallic acid (GA, 97.5 – 102.5%), pyrogallol (PG, 99.0%), pyrocatechol (PC, ≥99.0%), phloroglucinol (≥99.0%), phenol (≥99.0%), iron(III) chloride hexahydrate ($FeCl_3.6H_2O$), poly(ethyleneimine) (PEI, M_w = 25 kDa), poly(acrylic acid) (PAA, M_w = 10 kDa), sodium citrate, citric acid, glycine, sodium hydroxide (NaOH), and fluorescein isothiocyanate dextran (FITC-dextran) with various M_w (70, 250, 500, 2000 kDa) and *N*-methyl-2-pyrrolidone (NMP) were purchased from Sigma-Aldrich and used as received. Polystyrene (PS) particles (D = 3.55 ± 0.07μm), aminated silica particles (D = 3.07 ± 0.12 μm), melamine formaldehyde (MF) particles (D = 2.98 ± 0.06 μm) and poly(methyl methacrylate) (PMMA) particles (D = 3.67 ± 0.08 μm) were purchased from Microparticles GmbH. Poly(lactic acid) (PLA) particles (polydisperse), and poly(lactic-*co*-glycolic acid) (PLGA) particles (D = ~2 μm) were obtained from Corpuscular Inc. Tetrahydrofuran (THF) and acetone were purchased from Chem Supply. High-purity (Milli-Q) water with a resistivity of 18.2 MΩ cm was obtained from an inline Millipore RiOs/Origin water purification system.

Film Formation on Particulate Substrates. GA/Fe^{III} and PG/Fe^{III} Systems. The standard protocol is described as follows. 50 μL of polystyrene (PS, D = 3.55 ± 0.07, 10 wt% water suspension) particles was first washed twice with Milli-Q water. Then, 400 μL of the ligand (GA or PG) solution (15 mM) was added to the PS particles and vortexed for 10 s. 200 μL of $FeCl_3 \cdot 6H_2O$ (30 mM) solution was then added and quickly vortexed for 3-4 s. Subsequently, the mixture pH was raised by addition of 20 μL of 0.5 M NaOH solution, followed by vortexing for 1 min; the final pH values of the mixtures were ~3.8 and ~4.1 for the GA/Fe^{III} and PG/Fe^{III} systems, respectively. Unreacted supernatant was removed by centrifugation (1700 *g*, 1 min) followed by four washing steps in Milli-Q water. Dissolution of the PS cores was accomplished by washing the pellets with THF three times (1900 *g*, 1 min). The obtained hollow capsules were washed twice (2000 *g*, 3 min) with Milli-Q water and finally resuspended in 400 μL of Milli-Q water for characterization. Variation in the pH values of the film formation mixtures was also performed. For the GA/Fe^{III} system, stable film formation was observed within the pH range of 2.5 to 4.8. The pH values of the final mixtures in these cases were adjusted by adding small volumes of 0.1 M HCl or 0.1 M NaOH solutions. Coating GA/Fe^{III} on aminated-SiO_2, PMMA, PLA, or PLGA particles was performed in the same manner as described above, except that the PMMA and PLA particles were dissolved using 1:1 v/v acetone:NMP to obtain hollow capsules. Film formation (on PS particles) was also conducted by varying the starting concentrations of GA and Fe^{III} solutions from 7.5 to 20 mM, while keeping the pH and stoichiometry (ligand to metal 1:1) of the final mixture constant. For sequential assembly (multiple cycles) experiments, the standard film formation protocols described above were repeated.

PC/Fe^{III} System. The standard protocol is described as follows. Milli-Q water used for this system was degassed by N_2 bubbling for 15 min. 50 μL of polystyrene (PS, D = 3.55 ± 0.07, 10 wt% water suspension) particles was first washed twice with Milli-Q water. Then, 400 μL of PC solution (15 mM) was added to the PS particles and vortexed for 10 s. Subsequently, 200 μL of $FeCl_3 \cdot 6H_2O$ (30 mM) solution was added and the resultant mixture was vortexed for 1 min. Note that no additional pH adjustment is required for this system; the final pH value of the mixture was ~2.1. Unreacted supernatant was removed by centrifugation (1700 *g*, 1 min) and subsequent washing steps (four times) in Milli-Q water. Dissolution of the PS templates was accomplished by washing the pellets with THF three times (1900 *g*, 1 min). The obtained hollow capsules were washed twice (2000 *g*, 3 min) with Milli-Q water and finally resuspended in 400 μL of Milli-Q water for characterization. Variation in the pH values of the film formation mixtures was also performed. For the PC/Fe^{III} system, stable film formation was observed within the pH range of 1.8 to 2.4. The pH values of the final mixtures in these cases were adjusted by adding small volumes of 0.1 M HCl or 0.1 M NaOH solutions. Coating of aminated-SiO_2, PMMA, PLA, or PLGA particles was performed in the same manner as above, except that PMMA and PLA particles were dissolved in 1:1 v/v acetone:NMP to obtain hollow capsules. Film formation (on PS particles) was also conducted by varying the starting concentrations of PC and Fe^{III} solutions from 12.5 to 20 mM, while keeping stoichiometry (ligand to metal ratio as 1:1) of the final mixture constant. For sequential assembly (multiple cycles) experiments, the standard film formation protocols described above were repeated.

Film Formation on Planar Substrates. Substrates used for these experiments were PS, PDMS, and quartz, which were cut into suitable sized pieces. Piranha-cleaned quartz substrates were primed with a PEI layer by dipping the substrates in PEI (2 mg mL^{-1}, 0.5 M NaCl) solution for 15 min, rinsed in Milli-Q water and dried in N_2 flow. *Caution! Piranha solution is highly corrosive! Care should be taken during preparation.* Piranha-cleaned quartz substrates were also primed with a PEI/PAA bilayer by dipping the substrates alternately in PEI (2 mg mL^{-1}, 0.5 M NaCl) and PAA (2 mg mL^{-1}, 0.5 M NaCl) solution for 15 min with an intermediate rinsing (Milli-Q water) and drying (N_2) step. After applying the PAA layer the substrates were rinsed in Milli-Q water and dried in N_2 flow. PS and PDMS substrates were plasma treated to render them hydrophilic prior to GA/Fe^{III} or PC/Fe^{III} coating. Process parameters were maintained the same as the standard protocols used for the particulate coatings for both systems. For the GA/Fe^{III} system, a substrate was placed in a 15 mL tube and 4 mL of GA solution (15 mM) was added and vortexed for 10 s.

Subsequently 2 mL of $Fe^{III}Cl_3 \cdot 6H_2O$ (30 mM) solution was added and quickly vortexed for 3-4 s. 200 µL of 0.5 M NaOH solution was immediately added to the mixture and vortexed for 1 min. The substrate was then rinsed with Milli-Q water and dried with a N_2 stream. For the PC/Fe^{III} system, a substrate was placed in a 15 mL tube and 4 mL of PC solution (15 mM) was added and vortexed for 10 s. Subsequently 2 mL of $FeCl_3 \cdot 6H_2O$ (30 mM) solution was added and vortexed for 1 min. The substrate was then rinsed with Milli-Q water and dried with a N_2 stream. For both systems the coating processes were repeated three times to enhance the color difference. UV-Vis absorption spectra were recorded after each cycle for quartz substrates (primed with PEI) using a solid sample holder.

RESULTS AND DISCUSSION

Figure 1 gives an overview of the results obtained for the different phenolic ligands, showing the GA/Fe^{III}, PG/Fe^{III} and PC/Fe^{III} systems. Using particulate substrates, spherical freestanding films commonly known as capsules, were obtained after dissolving the templates in suitable solvents.[28] Particulate substrates are advantageous because film formation and stability can be examined immediately after their removal. GA/Fe^{III}, PG/Fe^{III} and PC/Fe^{III} capsules obtained using polystyrene (PS) particles as templates exhibited different colors (Figure 1b,d,f, respectively). UV-Vis absorption spectra for GA/Fe^{III}, PG/Fe^{III} and PC/Fe^{III} capsules (Figure 1g-i) showed maxima (λ_{max}) in the visible region around ~570 nm, ~619 nm, and ~680 nm, respectively. These bands are significantly different from the absorption bands of the ligands themselves, and likely arise from charge transfer (CT) bands,[29,30] which indicate the presence of metal-ligand coordination. Differential interference contrast (DIC) microscopy images of the corresponding systems showed stable and monodisperse capsules, which retained their spherical shape after template removal (Figure 1j-l). From microelectrophoresis measurements of these systems on PS particles, zeta (ζ)-potentials were found to be −39 ± 4, −38 ± 5, and −43 ± 6 mV for the GA/Fe^{III}, PG/Fe^{III} and PC/Fe^{III} systems, respectively. Bare PS particles showed a ζ-potential of −42 ± 5 mV. Generally, particles with ζ-potential values higher than ±30 mV are considered to be stable against agglomeration because of the strong repulsive forces among the particles.[31,32] Atomic force microscopy (AFM) performed on the air-dried capsules revealed surface features with folds and creases typical of collapsed capsule films (Figure 1m-o). Analyses of the collapsed flat regions of the GA/Fe^{III} and PC/Fe^{III} systems indicated smooth films with roughness values (rms) of ~0.3 and ~0.4 nm, respectively, whereas PG/Fe^{III} films showed a slightly rugged surface with a roughness value (rms) of ~1 nm. Single-wall film thicknesses from the AFM height profiles were determined to be 10.1 ± 0.5, 11.2 ± 0.8, and 11.4 ± 0.4 nm for GA/Fe^{III}, PG/Fe^{III}, and PC/Fe^{III} systems, respectively. Similar surface morphologies with folds and creases were observed by transmission electron microscopy (TEM) (Figure 1p-r). The presence of Fe^{III} ions in the films was confirmed by energy-dispersive X-ray spectroscopy (EDX) analyses (Figure S1).

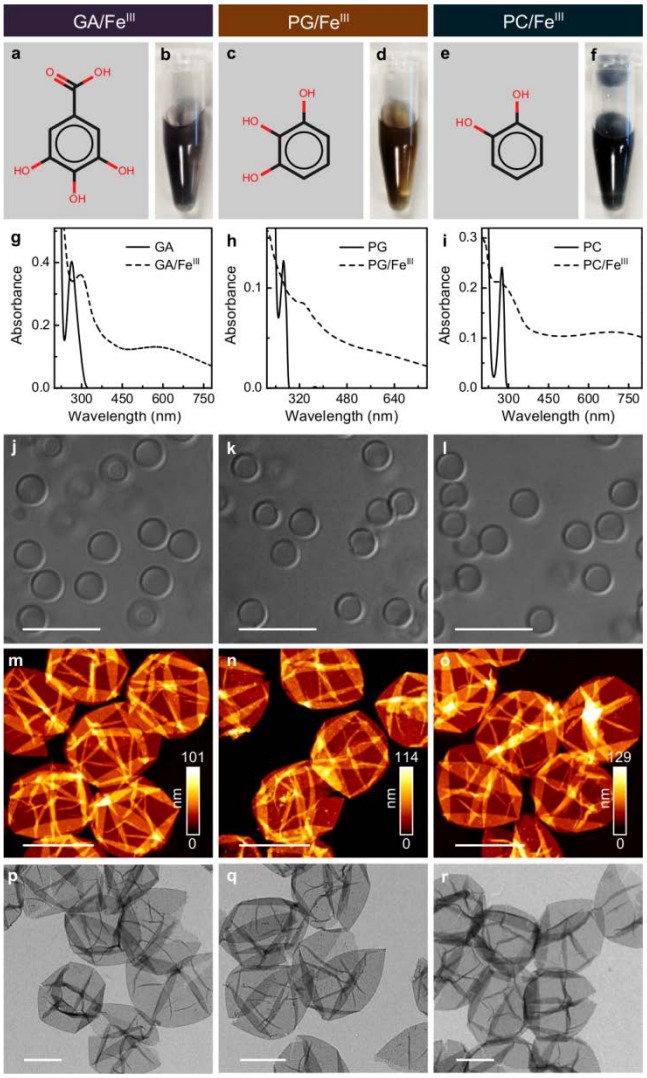

Figure 1. General characterization of GA/Fe^{III}, PG/Fe^{III}, and PC/Fe^{III} capsules. Each column represents one system. 2D structures of GA, PG, and PC (a, c, and e, respectively). Photographs (b, d, and f, respectively) showing capsule suspensions of GA/Fe^{III}, PG/Fe^{III}, and PC/Fe^{III} systems, respectively, in Milli-Q water. UV-Vis absorbance spectra showing the CT bands for the corresponding systems (g-i). Absorbance spectra of the ligand solutions are also presented for comparison. Aggregation-free, well-dispersed capsules are evident from the DIC images (j-l, scale bars correspond to 10 µm) for each system. AFM (m-o, scale bars correspond to 3 µm) and TEM (p-r, scale bars correspond to 2 µm) images correspond to the collapsed (dried) capsules for each system.

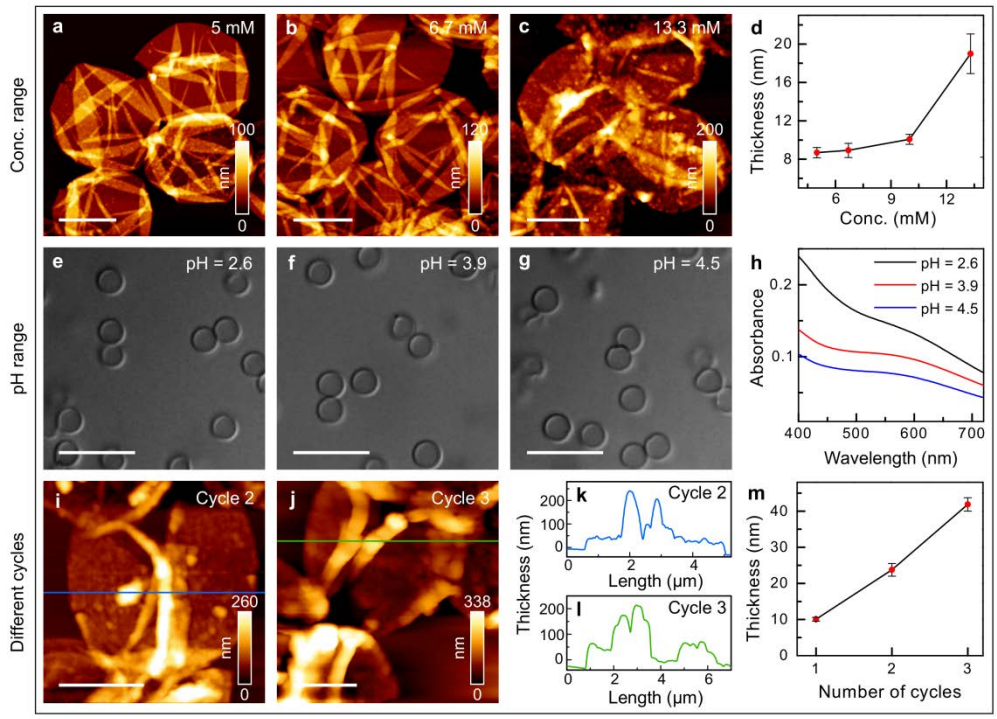

Figure 2. Characterization of the GA/Fe^{III} system with varying process parameters. AFM topographic images (a-c) of collapsed (dried) GA/Fe^{III} capsules at different starting concentrations of GA and Fe^{III} (GA:Fe^{III} = 1:1) showing surface morphologies of the capsules and the corresponding thicknesses, as measured by AFM height analyses (d). DIC images (e-g) of GA/Fe^{III} capsules prepared at different pH values of the mixture (GA and Fe^{III}) and the corresponding changes in the CT bands, as observed by UV-Vis absorption spectra (h). AFM topographic images (i, j) and height profiles (k, l)of collapsed (air-dried) GA/Fe^{III} capsules at different cycles showing surface morphologies of the capsules and the corresponding thicknesses, as measured by AFM height analyses (m) with different cycles. AFM scale bars correspond to 2 μm and DIC scale bars correspond to 10 μm.

Next, we focused on the GA/Fe^{III} and PC/Fe^{III} systems as the simplest model ditopic and monotopic chelating ligand (phenolic type) systems, respectively, to further examine the film formation process with different process parameters. Previous work has shown that GA and Fe^{III} form crystalline coordination frameworks.[33,34] This system thus allows an important comparison highlighting the differences in material structure (crystalline frameworks versus amorphous thin films) that results from varied assembly conditions (vide infra). Figure 2 displays the results of the GA/Fe^{III} film formation using different concentrations and pH conditions. The final concentrations of the ligand/metal varied from 5 mM to 13.3 mM while maintaining a [GA]:[Fe^{III}] stoichiometry of 1:1 The GA/Fe^{III} films formed showed a nonlinear trend of increasing thickness with increasing concentration. Smooth films were evident up to a concentration of 10 mM; however, at 13.3 mM the films became rougher and thicknesses increased to ~20 nm (Figure 2a-d). Alterations of the pH values of the mixture from 2.6 to 4.5 did not alter the stability of the capsules, as displayed by the DIC images of the stable capsules (Figure 2e-g). The CT bands in the UV-Vis absorption spectra showed slight red shifts with decreasing pH, accompanied by changes in the band shapes (Figure 2h). Repetition of the film formation cycle increased the film thicknesses from ~10 nm for the first cycle to ~40 nm for the third cycle (Figure 2i-m). Film formation was also studied on both planar and particulate substrates with different surface chemistries. Figure S2a-e (top panel) shows the film formation on different particulate templates, as is evident from the dark colored pellets after coating. DIC images of freestanding capsules obtained after poly(lactic acid) (PLA) and poly(methyl methacrylate) (PMMA) template removal are presented (Figure S2f,g, top panel). Photographs of GA/Fe^{III} films deposited on various planar supports such as PS, quartz, and polydimethylsiloxane (PDMS) are displayed in Figure S2a-d (bottom panel). The intensity of the CT band at ~570 nm increased with an increasing number of cycles on planar quartz substrates (Figure S2e, bottom panel). Similar experiments were performed on the PC/Fe^{III} system and presented in Figures S3 and S4. The concentration (8.3 to 13.3 mM) and pH (1.8 to 2.2) ranges for stable PC/Fe^{III} film formation were narrower than those for the GA/Fe^{III} system. An acidic pH for both systems was found to be crucial for film formation, which differs compared to the TA/Fe^{III} system, which forms films at pH 7.4.[19] GA and PC forms predominantly tris-type[29] complexes with Fe^{III} at basic pH and possibly such complexes are not suitable for extended network formation (vide infra).

Several properties, namely, disassembly, permeability, and Young's moduli (E_Y), of the GA/Fe^{III} and PC/Fe^{III} capsule systems were also investigated. Disassembly of GA/Fe^{III} and PC/Fe^{III} capsules dispersed in solutions with different pH values was monitored by following the decrease of CT band intensity over time (Figures 3a and S5). Over 90% of GA/Fe^{III} capsules disassembled within 10 min in solutions of pH 2

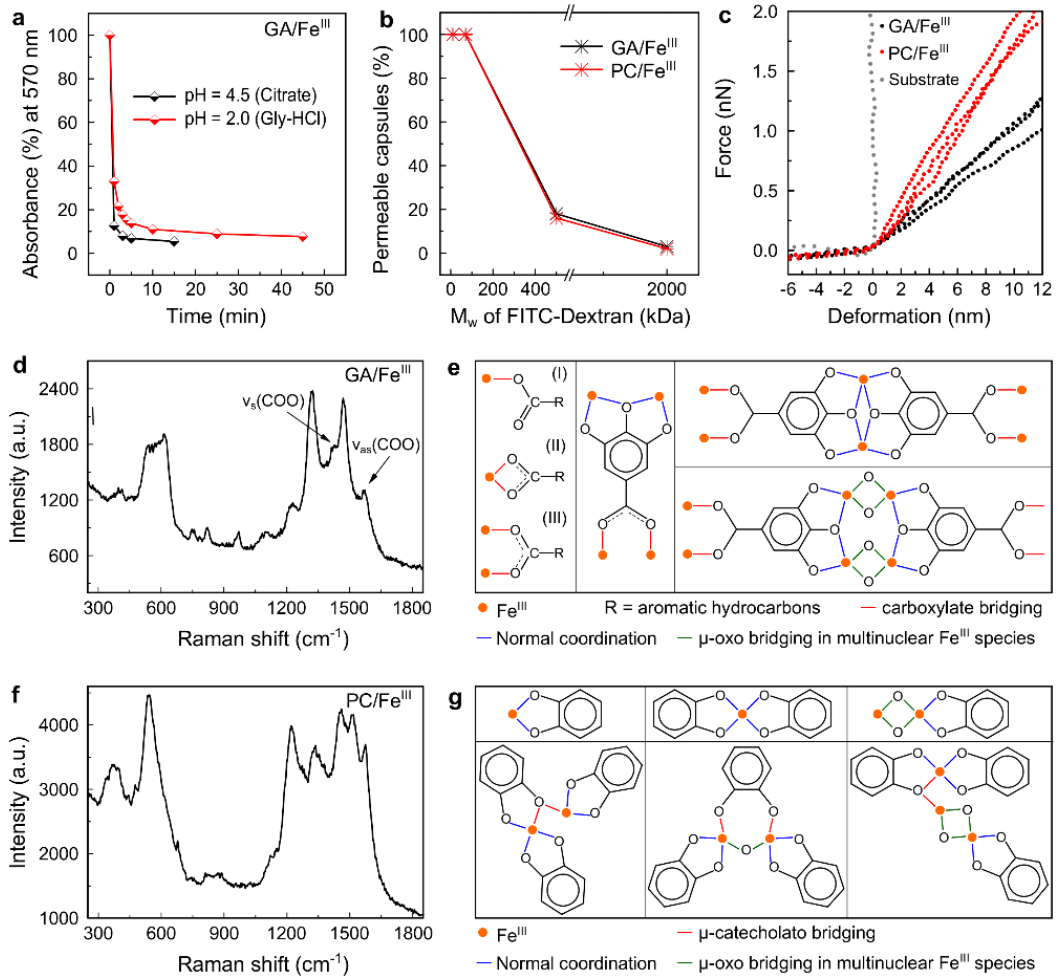

Figure 3. Properties and possible networks formation pathways of the GA/Fe^{III} and PC/Fe^{III} systems. Disassembly profile (a) for GA/Fe^{III} capsules monitored by UV-Vis absorption spectroscopy. Disassembly of the capsules was confirmed by DIC microscopy after the UV-Vis absorption experiments. Permeability (b) of GA/Fe^{III} and PC/Fe^{III} capsules with respect to different M_w of FITC-Dextran. Representative force-deformation curves (c) for the small deformation regime of GA/Fe^{III} (black) and PC/Fe^{III} (red) capsules. Force-deformation curve for hard substrate is also presented for comparison. RR spectra (d and f) of GA/Fe^{III} and PC/Fe^{III}, respectively. RR spectra were collected by an excitation wavelength of 782 nm. Different coordination modes for the –COOH group (e, left most column, i-iii) and galloyl group (the rest of e) of GA for the GA/Fe^{III} system (coordination modes are based on Refs. 33,34,53). Different coordination modes (g) for the vicinal diol group of PC in the PC/Fe^{III} system. Note that these coordination species have available binding sites (not shown) to form a large network/film. Coordinated H_2O molecules are omitted for clarity.

(glycine-HCl buffer) and pH 4.5 (citrate buffer), respectively (Figures 3a and S5a,b). In comparison, PC/Fe^{III} capsules showed over 70% disassembly when dispersed in solutions of pH 1.5 and pH 4.5 (citrate buffer) at 40 and 20 min (Figure S5c-e), respectively. Both types of capsules were permeable (Figure 3b) to 10 and 70 kDa FITC-dextran, and over 80% and 95% of the capsules were impermeable to 500 kDa and 2000 kDa FITC-dextran, respectively. The E_Y for GA/Fe^{III} and PC/Fe^{III} capsules were estimated to be 620 ± 200 MPa and 870 ± 240 MPa, respectively (Figure 3c) by AFM force measurements with a colloidal indenter. Comparing these values to the previously reported TA/Fe^{III} capsules (E_Y = 1 ± 0.2 GPa),[19] it is evident that both GA/Fe^{III} and PC/Fe^{III} capsules are less rigid than TA/Fe^{III} capsules. This difference is attributed to their different molecular structures and coordination modes during film formation.

As demonstrated, the three ligands (GA, PG and PC) were suitable to form free-standing films with distinct properties. However, attempts to form surface-confined films from a monodentate tritopic ligand (phloroglucinol, 1,3,5-trihydroxybenzene)) and a monodentate monotopic ligand (phenol) were unsuccessful. These results suggest that the presence of at least one vicinal diol group (i.e., bidentate) in the aromatic ring, as in PC, is a prerequisite for film formation (phenolic type ligand). It was hypothesized that metal-ligand coordination (vide infra) is the principal interaction mode for extended network and surface film formation. Thus the binding strength and stability of the complexes, and binding site availability to extend long range networks, were expected to be major factors influencing film formation. From the structures of phenol and phloroglucinol, we propose that the monodentate nature of these ligands does not favor a surface-confined film formation process.

The visual colors of the films and the CT bands suggest metal coordination as a major mode for the formation of the long range networks. The broadness of the CT bands further indicates the involvement of different types of coordination species (mono, bis, bridging, etc.) in films. To obtain better insight into the film formation process, X-ray photoelectron spectroscopy (XPS), resonance Raman (RR) spectroscopy and electrospray ionization mass spectrometry (ESI-MS) were employed. XPS data for GA/Fe^{III} and PC/Fe^{III} films revealed that the Fe $2p_{3/2}$ signal showed a main peak around ~712 eV with a 2p peak separation of ~14 eV, which is consistent with the presence of Fe^{III} being the dominant species in the films (Figure S6).[35] These results also indicate that the role of redox intermediates in the films is negligible (vide infra). RR spectra of pristine GA and PC (Figure S7) compared to GA/Fe^{III} and PC/Fe^{III} films (Figure 3d,f) respectively, revealed clear differences between pristine and coordinated forms of the ligands. Raman bands of the GA/Fe^{III} films at 1470, 1315, and 1230 cm^{-1} can be assigned to the skeletal modes of the substituted benzene ring.[36,37] Bands in the low frequency region of 650–500 (broad due to multiple peaks), and 400 cm^{-1} (very weak) can be attributed to the Fe-O vibration ($\nu_{Fe\text{-}O}$) arising from galloyl-Fe coordination.[36,37] Moreover, bands at 1570 (asymmetric, ν_{as}) and 1428 (symmetric, ν_s) cm^{-1} can be assigned to carboxylate (-COO)/Fe^{III} interactions, and the difference ($\Delta_{s\text{-}as}$) of these two bands of 142 cm^{-1} is consistent with the type(III) bridging mode of (-COO)/Fe^{III} interactions (Figure 3e).[38] Similarly, the RR spectrum of PC/Fe^{III} films (Figure 3f) showed features in the region of 1100–600 cm^{-1} arising from catechol ring vibrations, while the band at 533 cm^{-1} is characteristic of the catechol/Fe^{III} chelate ring mode.[39] An additional feature appeared around ~385 cm^{-1} (broad), which we tentatively assigned to the $\nu_{Fe\text{-}O}$ of μ-catecholato bridging mode. Considering an average Fe-O bond distance ($r_{Fe\text{-}O}$) of 2.1 Å in μ-catecholato bridging of Fe^{III}, Badger's rule predicts a $\nu_{Fe\text{-}O}$ at ~410 cm^{-1}.[40-42] Note that μ-catecholato/Fe^{III} bridging can also have different coordination modes with an average $r_{Fe\text{-}O}$ ranging from 1.87 to 2.18 Å, as observed earlier.[43] The slight discrepancy of bridging $\nu_{Fe\text{-}O}$ from Badger's rule in our system is most probably caused by different local environments around the Fe^{III} center in the film structure, which might increase the average bridging $r_{Fe\text{-}O}$ and shift the bridging $\nu_{Fe\text{-}O}$ to a lower frequency. We note that the existence of μ-oxo/hydroxo bridged di/multi-nuclear Fe^{III} species (due to hydrolysis of Fe^{III} in aqueous solution) in the films may occur, but would be difficult to detect experimentally.[44]

Transition metal-induced oxidative di- or oligomerization of phenolic compounds via *o*-quinone/semiquinone intermediate formation is well established in literature.[45,46] However, the extent of this process is dependent on several factors, including metal-to-ligand stoichiometry and concentration, reaction pH, and most importantly, reaction time.[47-49] In this study, the PC/Fe^{III} system is more vulnerable to this process. Three possibilities can be considered for this system during film formation: 1) PC dimers or higher oligomers are formed initially and later form films through coordinative crosslinking; 2) initially formed PC dimers or higher oligomers, along with PC monomers, formed films through coordinative crosslinking where PC dimers or higher oligomers have a significant contribution to film formation; and 3) PC monomers form films through coordinative crosslinking where PC dimers or higher oligomers have negligible contribution to the film formation. To probe these possibilities, we studied the PC/Fe^{III} complexes in solution (identical conditions used to those for film formation) over time by ESI-MS in negative ion mode (Figure S8). The first measurement was taken at t = 2.5 min from the time of mixing (t = 0). A negligible amount (~0.4%) of PC dimers (*m/z* 217.05) was observed at this time point period, which increased only marginally (~1.5%) at t = 23 min compared to the PC monomeric peak (*m/z* 109.03). Higher oligomeric species were not observed in this timeframe. Therefore, considering the film formation time of 1 min, the first two possibilities for the PC/Fe^{III} system, described above, can largely be excluded, leaving metal coordination with monomeric ligand species as the dominant driver for film formation. Furthermore, negligible covalent crosslinking was observed in several other studies[50-52] during coordinative gel formation of catechol containing polymers with Fe^{III}, although the timeframes in those studies were much longer (from 1–12 h). For the GA/Fe^{III} system, ESI-MS analyses were performed after disassembling the capsules into their molecular fragments by concentrated HCl treatment. Organic fragments of the GA/Fe^{III} system appeared as a prominent peak at *m/z* 169.01 attributed to monomeric GA (Figure S9). Other major peaks observed can be assigned to iron-chloride adducts, as evidenced by their corresponding isotopic patterns. Importantly, no dimeric (*m/z* 337.02) or oligomeric GA species were detected. Similar results were obtained for the PG/Fe^{III} system with the absence of any dimeric or oligomeric PG species.

From the above investigations, network formation in the GA/Fe^{III} and PC/Fe^{III} systems can be viewed in the following manner. For the GA/Fe^{III} system, carboxylic and hydroxyl groups of GA provide sufficient binding sites for mono and multinuclear Fe^{III} species to form a large network by different coordination modes,[33,34,38,53] as displayed in Figure 3e. For the PC/Fe^{III} system, the vicinal diol groups of PC act as mono and bi-dentate ligands, where the bidentate nature gives rise to mono- and bis-type local complexes[29,30] with mono and multinuclear Fe^{III} species, and the monodentate nature provides the bridging[40,41] of these complexes allowing network formation (Figure 3g). The dark green coloration of PC-Fe^{III} complexes usually arises from the formation of mono-type complexes. These discrete complexes are susceptible to redox reactions and discoloration occurs over time by formation of *o*-quinone/semiquinone intermediates (as mentioned above). In this case, the color of the PC/Fe^{III} capsules (bluish dark green) remained unchanged over 7 days, suggesting that the mono-type complexes present in the films were not discrete entities, but parts of an extended network.

The absence (or negligible presence) of covalent interactions suggests that film formation is a generic coordination phenomenon of phenolic ligand-metal interactions at the solid-liquid interface. Interestingly, phenolic ligand/metal pairs are also able to form crystalline framework materials in solution, when phenolic ligands with divergent chelating sites (i.e., ditopic), such as GA, are used. However, formation of crystalline framework materials in solution or surface-confined amorphous films at the solid-liquid interface occurs with different kinetics and under different process parameters. One example is the GA/Fe^{III} system, which allows for the production of GA/Fe^{III} MOFs and films (Figure 4a,b). GA/Fe^{III} MOFs were produced following a published protocol.[34] Figure 4c-f displays the differences between the two systems

containing identical structural components. The SEM image of GA/Fe^{III} MOFs showed needles with crystalline features whereas GA/Fe^{III} films showed amorphous features with folds and creases (Figure 4c,d).

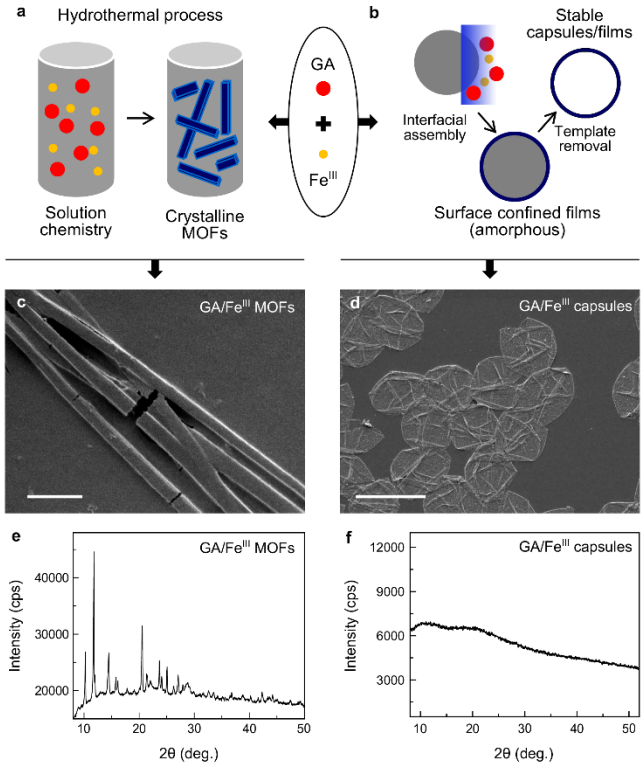

Figure 4. Comparison of the GA/Fe^{III} MOFs and GA/Fe^{III} capsules. Schematic showing formation of (a) crystalline and (b) amorphous materials by GA/Fe^{III} interaction in different conditions. SEM and XRD characterization of GA/Fe^{III} MOFs (c, e) and GA/Fe^{III} capsules (d, f), respectively. Scale bars correspond to 2 µm and 3 µm for c and d, respectively.

XRD patterns further support this variation in the supramolecular phases of the two systems, where the periodic arrangements of atoms in the GA/Fe^{III} MOFs caused prominent Bragg peaks (consistent with the published values)[33,34] and the aperiodic arrangements of atoms in the GA/Fe^{III} films resulted in broad humps caused by diffuse scattering (Figure 4e,f). Conceptually, these amorphous films are likely to form by a rapid, kinetically dominated non-equilibrium process, while crystalline MOFs are known to form in a slow, kinetically reversible and thermodynamically controlled manner.[1,3] The thermodynamic and kinetic aspects of these phenolic/metal pairs in producing different stable phases (crystalline and amorphous) may provide fundamental insights into the interfacial and solution phase chemistry of coordination complexes, and require further detailed investigations.

CONCLUSION

In conclusion, we have demonstrated a simple, rapid and generic surface-confined film formation strategy by utilizing coordination-driven self-assembly of simple phenolic building blocks, such as gallic acid, pyrogallol and pyrocatechol. The structural simplicity of the ligands allowed for a more in-depth evaluation of their contribution to the film formation process. These molecular hybrid films might provide a versatile multifunctional platform for a range of applications, including catalysis, energy and optoelectronics. Moreover, the biological relevance of the phenolic ligands, combined with the dynamic metal-ligand interactions, may make them of interest in the biomedical sciences.

ASSOCIATED CONTENT

Supporting Information. Details of characterization methods, detailed experimental protocols for film disassembly, permeability, mechanical testing, ESI-MS analyses of the organic fragments of disassembled capsules, synthesis of GA/Fe^{III} MOF crystals. EDX spectra of GA/Fe^{III}, PG/Fe^{III}, and PC/Fe^{III} systems, photographs of GA/Fe^{III} films on various templates, characterization of the PC/Fe^{III} system with varying process parameters, photographs of PC/Fe^{III} films on various templates, UV-Vis absorbance spectra to determine disassembly kinetics of GA/Fe^{III} and PC/Fe^{III} systems, XPS spectra of a GA/Fe^{III} and PC/Fe^{III} systems, RR spectra of GA and PC, time dependent ESI-MS spectra of PC/Fe^{III} complex solution, and ESI-MS spectra of disassembled GA/Fe^{III} and PG/Fe^{III} capsules. This material is available free of charge via the Internet at http://pubs.acs.org.

AUTHOR INFORMATION

Corresponding Author

* Tel.: +61 3 8344 3461. Fax: +61 3 8344 4153. E-mail: fcaruso@unimelb.edu.au.

Present Addresses

§ Department of Chemistry, University of Warwick, Coventry, CV4 7AL, UK.
¶ Institute of Industrial Science, The University of Tokyo, 4-6-1 Komaba, Meguro-ku, Tokyo, Japan.
# School of Chemistry, The University of Sydney, NSW 2006, Australia.

Author Contributions

The manuscript was written through contributions of all authors. All authors have given approval to the final version of the manuscript. The authors declare no competing financial interest.

Funding Sources

This research was funded by the Australian Research Council Centre of Excellence in Convergent Bio-Nano Science and Technology (project number CE140100036). This work was also supported by the Australian Research Council under the Australian Laureate Fellowship (F.C., FL120100030) scheme.

ACKNOWLEDGMENTS

M.A.R. acknowledges funding from the Australian Government through an International Postgraduate Research Scholarship (IPRS) and an Australian Postgraduate Award (APA). M.M. acknowledges The University of Melbourne for a McKenzie Fellowship. K.K. is grateful to the Alexander von Humboldt Foundation (Feodor-Lynen Fellowship) for financial support. We also acknowledge Dr. Kwun Lun Cho for XPS measurements. This work was performed in part at the Materials Characterisation

and Fabrication Platform (MCFP) at The University of Melbourne and the Victorian Node of the Australian National Fabrication Facility (ANFF).

ABBREVIATIONS

AFM, atomic force microscopy; CT, charge transfer; GA, gallic acid; MOF, metal organic framework; PC, pyrocatechol; PG, pyrogallol.

REFERENCES

(1) Chakrabarty, R.; Mukherjee, P. S.; Stang, P. J. Supramolecular Coordination: Self-Assembly of Finite Two- and Three-Dimensional Ensembles. *Chem. Rev.* **2011**, *111*, 6810-6918.

(2) Lehn, J. M. *Supramolecular Chemistry: Concepts and Perspectives*; VCH: Weinheim, Germany, 1995.

(3) Cook, T. R.; Zheng, Y.-R.; Stang, P. J. Metal-Organic Frameworks and Self-Assembled Supramolecular Coordination Complexes: Comparing and Contrasting the Design, Synthesis, and Functionality of Metal-Organic Materials. *Chem. Rev.* **2013**, *113*, 734-77.

(4) Hoskins, B. F.; Robson, R. Infinite Polymeric Frameworks Consisting of Three Dimensionally Linked Rod-Like Segments. *J. Am. Chem. Soc.* **1989**, *111*, 5962-5964.

(5) Gable, R. W.; Hoskins, B. F.; Robson, R. A New Type of Interpenetration Involving Enmeshed Independent Square Grid Sheets. The Structure of Diaquabis-(4,4'-bipyridine)zinc Hexafluorosilicate. *J. Chem. Soc., Chem. Commun.* **1990**, 1677-1678.

(6) Foo, M. L.; Matsuda, R.; Kitagawa, S. Functional Hybrid Porous Coordination Polymers. *Chem. Mater.* **2014**, *26*, 310-322.

(7) Yaghi, O. M.; O'Keeffe, M.; Ockwig, N. W.; Chae, H. K.; Eddaoudi, M.; Kim, J. Reticular Synthesis and the Design of New Materials. *Nature* **2003**, *423*, 705-714.

(8) Eddaoudi, M.; Kim, J.; Rosi, N.; Vodak, D.; Wachter, J.; O'Keeffe, M.; Yaghi, O. M. Systematic Design of Pore Size and Functionality in Isoreticular MOFs and Their Application in Methane Storage. *Science* **2002**, *295*, 469-472.

(9) Rosi, N. L.; Eckert, J.; Eddaoudi, M.; Vodak, D. T.; Kim, J.; O'Keeffe, M.; Yaghi, O. M. Hydrogen Storage in Microporous Metal-Organic Frameworks. *Science* **2003**, *300*, 1127-1129.

(10) Matsuda, R.; Kitaura, R.; Kitagawa, S.; Kubota, Y.; Belosludov, R. V.; Kobayashi, T. C.; Sakamoto, H.; Chiba, T.; Takata, M.; Kawazoe, Y.; Mita, Y. Highly Controlled Acetylene Accommodation in a Metal-Organic Microporous Material. *Nature* **2005**, *436*, 238-241.

(11) Kreno, L. E.; Leong, K.; Farha, O. K.; Allendorf, M.; Van Duyne, R. P.; Hupp, J. T. Metal–Organic Framework Materials as Chemical Sensors. *Chem. Rev.* **2012**, *112*, 1105-1125.

(12) Furukawa, H.; Cordova, K. E.; O'Keeffe, M.; Yaghi, O. M. The Chemistry and Applications of Metal-Organic Frameworks. *Science* **2013**, *341*, 1230444.

(13) Wang, C.; Liu, D.; Lin, W. Metal–Organic Frameworks as a Tunable Platform for Designing Functional Molecular Materials. *J. Am. Chem. Soc.* **2013**, *135*, 13222-13234.

(14) Tang, Z.; Wang, Y.; Podsiadlo, P.; Kotov, N. A. Biomedical Applications of Layer-by-Layer Assembly: From Biomimetics to Tissue Engineering. *Adv. Mater.* **2006**, *18*, 3203-3224.

(15) Srivastava, S.; Kotov, N. A. Composite Layer-by-Layer (LBL) Assembly with Inorganic Nanoparticles and Nanowires. *Acc. Chem. Res.* **2008**, *41*, 1831-1841.

(16) Liu, Y.; Ai, K.; Lu, L. Polydopamine and Its Derivative Materials: Synthesis and Promising Applications in Energy, Environmental, and Biomedical Fields. *Chem. Rev.* **2014**, *114*, 5057-5115.

(17) Sanchez, C.; Belleville, P.; Popall, M.; Nicole, L. Applications of Advanced Hybrid Organic-Inorganic Nanomaterials: From Laboratory to Market. *Chem. Soc. Rev.* **2011**, *40*, 696-753.

(18) Shi, J.; Jiang, Y.; Wang, X.; Wu, H.; Yang, D.; Pan, F.; Su, Y.; Jiang, Z. Design and Synthesis of Organic-Inorganic Hybrid Capsules for Biotechnological Applications. *Chem. Soc. Rev.* **2014**, *43*, 5192-5210.

(19) Ejima, H.; Richardson, J. J.; Liang, K.; Best, J. P.; van Koeverden, M. P.; Such, G. K.; Cui, J.; Caruso, F. One-Step Assembly of Coordination Complexes for Versatile Film and Particle Engineering. *Science* **2013**, *341*, 154-157.

(20) Guo, J.; Ping, Y.; Ejima, H.; Alt, K.; Meissner, M.; Richardson, J. J.; Yan, Y.; Peter, K.; von Elverfeldt, D.; Hagemeyer, C. E.; Caruso, F. Engineering Multifunctional Capsules through the Assembly of Metal–Phenolic Networks. *Angew. Chem., Int. Ed.* **2014**, *126*, 5652-5657.

(21) Ping, Y.; Guo, J.; Ejima, H.; Chen, X.; Richardson, J. J.; Sun, H.; Caruso, F. Ph-Responsive Capsules Engineered from Metal–Phenolic Networks for Anticancer Drug Delivery. *Small* **2015**, *11*, 2032-2036.

(22) Park, J. H.; Kim, K.; Lee, J.; Choi, J. Y.; Hong, D.; Yang, S. H.; Caruso, F.; Lee, Y.; Choi, I. S. A Cytoprotective and Degradable Metal–Polyphenol Nanoshell for Single-Cell Encapsulation. *Angew. Chem., Int Ed.* **2014**, *53*, 12420-12425.

(23) Ju, Y.; Cui, J.; Müllner, M.; Suma, T.; Hu, M.; Caruso, F. Engineering Low-Fouling and pH-Degradable Capsules through the Assembly of Metal-Phenolic Networks. *Biomacromolecules* **2015**, *16*, 807-814.

(24) Stock, N.; Biswas, S. Synthesis of Metal-Organic Frameworks (MOFs): Routes to Various MOF Topologies, Morphologies, and Composites. *Chem. Rev.* **2012**, *112*, 933-969.

(25) Vuong, G.-T.; Pham, M.-H.; Do, T.-O. Direct Synthesis and Mechanism of the Formation of Mixed Metal Fe_2Ni-MIL-88B. *CrystEngComm* **2013**, *15*, 9694-9703.

(26) Bennett, T. D.; Cheetham, A. K. Amorphous Metal–Organic Frameworks. *Acc. Chem. Res.* **2014**, *47*, 1555-1562.

(27) Deria, P.; Mondloch, J. E.; Karagiaridi, O.; Bury, W.; Hupp, J. T.; Farha, O. K. Beyond Post-Synthesis Modification: Evolution of Metal-Organic Frameworks Via Building Block Replacement. *Chem. Soc. Rev.* **2014**, *43*, 5896-5912.

(28) Caruso, F.; Caruso, R. A.; Möhwald, H. Nanoengineering of Inorganic and Hybrid Hollow Spheres by Colloidal Templating. *Science* **1998**, *282*, 1111-1114.

(29) Sever, M. J.; Wilker, J. J. Visible Absorption Spectra of Metal-Catecholate and Metal-Tironate Complexes. *Dalton Trans.* **2004**, 1061-1072.

(30) Perron, N. R.; Brumaghim, J. L. A Review of the Antioxidant Mechanisms of Polyphenol Compounds Related to Iron Binding. *Cell Biochem Biophys* **2009**, *53*, 75-100.

(31) Clogston, J. D.; Patri, A. K. In *Characterization of Nanoparticles Intended for Drug Delivery*; McNeil, S. E., Ed.; Humana Press: New York, NY, 2011; Chapter 6, pp 63-70.

(32) Hunter, R. J. *Zeta Potential in Colloid Science: Principles and Applications*; Academic Press: London, United Kingdom, 1981.

(33) Wunderlich, C.-H.; Weber, R.; Bergerhoff, G. Über Eisengallustinte. *Z. Anorg. Allg. Chem.* **1991**, *598*, 371-376.

(34) Feller, R. K.; Cheetham, A. K. Fe(III), Mn(II), Co(II), and Ni(II) 3,4,5-Trihydroxybenzoate (Gallate) Dihydrates; a New Family of Hybrid Framework Materials. *Solid State Sci.* **2006**, *8*, 1121-1125.

(35) Moulder, J. F.; Stickle, W. F.; Sobol, P. E.; Bomben, K. D. *Handbook of X-Ray Photoelectron Spectroscopy: A Reference Book of Standard Spectra for Identification and Interpretation of XPS Data*; Physical Electronics: Eden Prairie, MN, 1995.

(36) Salama, S.; Stong, J. D.; Neilands, J. B.; Spiro, T. G. Electronic and Resonance Raman Spectra of Iron(III) Complexes of Enterobactin, Catechol, and *N*-Methyl-2,3-dihydroxybenzamide. *Biochemistry* **1978**, *17*, 3781-3785.

(37) Lee, A. S.; Mahon, P. J.; Creagh, D. C. Raman Analysis of Iron Gall Inks on Parchment. *Vib. Spectrosc.* **2006**, *41*, 170-175.

(38) Nakamoto, K. *Infrared and Raman Spectra of Inorganic and Coordination Compounds, Applications in Coordination, Organometallic, and Bioinorganic Chemistry*; John Wiley & Sons, Inc.: Hoboken, NJ, 2009.

(39) Michaud-Soret, I.; Andersson, K. K.; Que, L., Jr.; Haavik, J. Resonance Raman Studies of Catecholate and Phenolate Complexes

of Recombinant Human Tyrosine Hydroxylase. *Biochemistry* **1995**, *34*, 5504-5510.

(40) Grillo, V. A.; Hanson, G. R.; Wang, D.; Hambley, T. W.; Gahan, L. R.; Murray, K. S.; Moubaraki, B.; Hawkins, C. J. Synthesis, X-Ray Structural Determination, and Magnetic Susceptibility, Mössbauer, and EPR Studies of $(Ph_4P)_2[Fe_2(Cat)_4(H_2O)_2]\cdot 6H_2O$, a Catecholato-Bridged Dimer of Iron(III). *Inorg. Chem.* **1996**, *35*, 3568-3576.

(41) Boudalis, A. K.; Dahan, F.; Bousseksou, A.; Tuchagues, J.-P.; Perlepes, S. P. Use of the Di-2-pyridyl Ketone/3,5-Di-*tert*-butylcatechol "Blend" in Iron(III) Chemistry: A Cationic Tetranuclear Cluster and an Anionic Trinuclear Complex. *Dalton Trans.* **2003**, 3411-3418.

(42) Green, M. T. Application of Badger's Rule to Heme and Non-Heme Iron−Oxygen Bonds: An Examination of Ferryl Protonation States. *J. Am. Chem. Soc.* **2006**, *128*, 1902-1906.

(43) Boone, S. R.; Purser, G. H.; Chang, H.-R.; Lowery, M. D.; Hendrickson, D. N.; Pierpont, C. G. Magnetic Exchange Interactions in Semiquinone Complexes of Iron. Structural and Magnetic Properties of Tris(3,5-di-*tert*-butylsemiquinonato)iron(III) and Tetrakis(3,5-di-*tert*-butylsemiquinonato)tetrakis(3,5-di-*tert*-butylcatecholato)tetrairon(III). *J. Am. Chem. Soc.* **1989**, *111*, 2292-2299.

(44) Taylor, S. W.; Chase, D. B.; Emptage, M. H.; Nelson, M. J.; Waite, J. H. Ferric Ion Complexes of a Dopa-Containing Adhesive Protein from *Mytilus Edulis*. *Inorg. Chem.* **1996**, *35*, 7572-7577.

(45) Barrett, D. G.; Sileika, T. S.; Messersmith, P. B. Molecular Diversity in Phenolic and Polyphenolic Precursors of Tannin-Inspired Nanocoatings. *Chem. Commun.* **2014**, *50*, 7265-7268.

(46) Fullenkamp, D. E.; Barrett, D. G.; Miller, D. R.; Kurutz, J. W.; Messersmith, P. B. pH-Dependent Cross-Linking of Catechols through Oxidation Via Fe^{3+} and Potential Implications for Mussel Adhesion. *RSC Adv.* **2014**, *4*, 25127-25134.

(47) Mentasti, E.; Pelizzetti, E. Reactions between Iron(III) and Catechol (*O*-Dihydroxybenzene). Part I. Equilibria and Kinetics of Complex Formation in Aqueous Acid Solution. *J. Chem. Soc., Dalton Trans.* **1973**, 2605-2608.

(48) Zeng, H.; Hwang, D. S.; Israelachvili, J. N.; Waite, J. H. Strong Reversible Fe^{3+}-Mediated Bridging between Dopa-Containing Protein Films in Water. *Proc. Natl. Acad. Sci. U.S.A* **2010**, *107*, 12850-12853.

(49) Yang, J.; Cohen Stuart, M. A.; Kamperman, M. Jack of All Trades: Versatile Catechol Crosslinking Mechanisms. *Chem. Soc. Rev.* **2014**, *43*, 8271-8298.

(50) Holten-Andersen, N.; Harrington, M. J.; Birkedal, H.; Lee, B. P.; Messersmith, P. B.; Lee, K. Y. C.; Waite, J. H. Ph-Induced Metal-Ligand Cross-Links Inspired by Mussel Yield Self-Healing Polymer Networks with near-Covalent Elastic Moduli. *Proc. Nat. Acad. Sci. U.S.A* **2011**, *108*, 2651-2655.

(51) Ceylan, H.; Urel, M.; Erkal, T. S.; Tekinay, A. B.; Dana, A.; Guler, M. O. Mussel Inspired Dynamic Cross-Linking of Self-Healing Peptide Nanofiber Network. *Adv. Funct. Mater.* **2013**, *23*, 2081-2090.

(52) Yavvari, P. S.; Srivastava, A. Robust, Self-Healing Hydrogels Synthesised from Catechol Rich Polymers. *J. Mat. Chem. B* **2015**, *3*, 899-910.

(53) Senvaitiene, J.; Beganskiene, A.; Kareiva, A. Spectroscopic Evaluation and Characterization of Different Historical Writing Inks. *Vib. Spectrosc.* **2005**, *37*, 61-67.

Table of Contents Only